Fluorescence Quenching in a Strongly Helical Peptide Series: The Role of Noncovalent Pathways in Modulating Electronic Interactions†

Gautam Basu, Demetrios Anglos, and Atsuo Kuki*

Baker Laboratory, Department of Chemistry, Cornell University, Ithaca, New York 14853

Received September 15, 1992; Revised Manuscript Received January 19, 1993

ABSTRACT: The very strong helical propensity of peptides rich in α-aminoisobutyric acid (Aib) has enabled the design of a set of helices containing as guest amino acids one fluorescent chromophore, β-(1′-naphthyl)-L-alanine, and one heavy atom perturber, *p*-bromo-L-phenylalanine. The fluorescence of the chromophoric residue was monitored in this set to explore heavy atom induced enhanced intersystem crossing as a potentially useful tool for exploring remote electronic interactions in biomolecules. The peptides in this set were sequence isomers of each other and were designed such that the chromophore and the perturber were separated by two, one, or zero Aib residues. The respective distances between the aromatic side chains are then modulated by the twist of the helix. All peptides showed steady-state fluorescence quenching, and on the basis of further time-resolved triplet–triplet absorption experiments, two mechanisms for the heavy atom induced fluorescence quenching were established: (i) a weak and nominally spin-forbidden singlet–triplet energy transfer and (ii) the remote heavy atom effect (RHAE) on the intersystem crossing within the fluorophore. Both the rate of singlet–triplet energy-transfer and the RHAE are at their maxima in the peptide with the largest sequence separation but the smallest direct distance between the chromophore and the perturber. Thus neither quenching mechanism is controlled by the length of the intervening covalent pathway. Subtle factors arising from the structure of the intervening peptide backbone apparently contribute to the RHAE for the peptides with shorter sequence separation. Because the sensitivity to the remote heavy atom is a measure of electronic delocalization, this result may have significance for the understanding of the role of helices in biological electron-transfer interactions.

In order to understand the complex nature of long-range electron transfer in proteins, several recent experimental studies have focused on the systematic examination of the quantum electronic delocalization between two interacting partners in peptide systems designed to have simpler molecular architectures than proteins. These weak electronic interactions across the peptide frame lead to peptide-mediated quenching processes whose quantitative measurement enables the precise analysis of electronic interactions within a single secondary structural element. One prominent approach relies upon oligoproline peptide spacers (DeFellips et al., 1990; Schanze et al., 1990; Isied et al., 1992) to separate the two interacting partners. An alternative design, used in the present work, is to synthesize helical polypeptides in which the interacting partners are themselves guest amino acids within the sequence (Basu et al., 1990; Sisido et al., 1989; Inai et al., 1990); this differs from the more common spacer approach in that the interacting partners are positioned within the region of maximum conformational rigidity, and the partners do not occur as end-capping groups. While a more or less exponential distance dependence of electron-transfer rate has been observed in the polyproline systems, the question of the degree to which electronic couplings are modulated by covalent bonded pathways or noncovalent electronic interactions is yet to be unequivocally established. Molecular systems based on the spacer strategy to separate the interacting partners show a strong correlation between through-bond (TB)[1] separation and the observed electronic interaction (Isied et al., 1992), whereas in structures where the interacting partners are incorporated within the sequence as modified amino acids, the evidence so far indicates a different pattern which is the correlation of electronic couplings with through-space (TS) separation (Basu et al., 1990; Sisido et al., 1989; Inai et al., 1990). In proteins, due to the complex three-dimensional nature of the backbone fold, numerous alternative and parallel pathways for electron transfer may become available based on combinations of TB and TS couplings. In order to quantitatively understand the role of the intervening medium in controlling the electron-transfer kinetics, discriminating experimental evidence on the fundamental origin of remote electronic interactions and on the relative contributions of the covalent vs noncovalent mechanisms is required.

Several theoretical approaches toward an understanding of electron-transfer pathways in proteins have been reported (Kuki & Wolynes, 1987; Kuki, 1991; Beratan et al., 1991; Christensen et al., 1990; Broo & Larsson, 1991; Siddharth & Marcus, 1990), and currently work toward this goal is being pursued in this laboratory (Gruchus & Kuki, 1992). Across this broad range of theoretical models, hydrogen bonds inevitably appear as important links in the network of the intervening protein matrix. Experimental approaches based on synthetic molecules of intermediate complexity—where, by synthetic design, the types of pathways available for electron

† This work was supported by the NIHGMS First Program (R29-GM39576). A.K. also acknowledges support from the NSF Presidential Young Investigator Program (CHEM-8958514) and the Camille and Henry Dreyfus Foundation (TS-89-12).

[1] Abbreviations: TS, through-space; TB, through-bond; RHAE, remote heavy atom effect; Aib, α-aminoisobutyric acid; Nap, β-(1′-naphthyl)-L-alanine; Bph, *p*-bromophenylalanine; Phe, phenylalanine; MNap, 1-methylnaphthalene; BrBz, bromobenzene; ISC, intersystem crossing; NMR, nuclear magnetic resonance; FAB-MS, fast atom bombardment mass spectroscopy; HPLC, high-performance liquid chromatography; ROESY, rotating frame Overhauser effect spectroscopy; NOE, nuclear Overhauser effect; ROE, rotating frame Overhauser effect; DMSO, dimethyl sulfoxide; ϕ_F, fluorescence yield; ϕ_T, triplet yield.

0006-2960/93/0432-3067$04.00/0

transfer can be controlled—should also retain essential structural attributes of the native proteins. For example, α-helices (Sisido et al., 1989; Inai et al., 1990) and 3_{10} helices (Basu et al., 1990) feature the hydrogen-bonded helical backbone, whereas oligoproline has no hydrogen bonds at all. Molecules where the interacting partners are covalently attached to the termini of spacer units (DeFellips et al., 1990; Schanze et al., 1990; Isied et al., 1992) also cannot address the question of the relative contribution of noncovalent vs covalent interactions toward remote electronic interactions, since with a change in the number of spacer units both the TS and the TB separations change monotonically. As a consequence their relative contribution remains entangled throughout the series. This problem can be circumvented if the partners can be incorporated as the side chains of modified amino acids within a peptide featuring a helical secondary structure. As the two partners in such a peptide system are synthetically moved further apart in sequence, the TB distance increases monotonically whereas the TS distance is modulated by the pitch of the helix (see Figure 1).

In a previous report (Basu et al., 1990), we demonstrated a remote heavy atom effect (RHAE) which is the enhancement of intersystem crossing in a chromophore due to the presence of a remote heavy atom. In a peptide environment, this RHAE can be operative between the chromophore and the heavy atom perturber even when the two partners are separated by 13 σ bonds of the helical backbone. The extreme sensitivity of the remote heavy atom induced fluorescence quenching to the inter-residue electronic interaction and the fact that the nature of the electronic coupling between the two partners in the case of RHAE is, in principle, closely related to the electronic coupling involved in nonadiabatic electron transfer allow one to apply results obtained from RHAE studies to the mechanistic elucidation of electron transfer. Both processes require particle exchange between the two components as opposed to, for example, Förster resonance excitation transfer (Förster, 1948). Similar connections between electron transfer and Dexter-type (Dexter, 1953) triplet–triplet energy transfer have been demonstrated experimentally (Closs et al., 1988). Furthermore, in contrast to electron transfer, the solvent and nuclear reorganizations associated with the transitions between the neutral excited states are relatively slight, making it easier to focus exclusively on the role of electronic coupling. It is this electronic coupling matrix element that is central to revealing the quantum mechanical role of the intervening medium in enabling remote electronic interactions.

In this article, we report our investigations on a series of helical peptides containing the naphthyl chromophore and the *p*-bromophenyl heavy atom perturber, which are incorporated as side chains of guest residues systematically placed along oligopeptides rich in the host α-aminoisobutyric acid (Aib) residue. The peptides were designed to contain the amino acid Aib so that the available conformational space becomes restricted to a narrow helical region due to the presence of the α,α-dimethyl in Aib (Prasad & Balaram, 1984; Karle & Balaram, 1990; Marshall et al., 1990; Toniolo et al., 1984). The peptides were composed of six Aib residues, the chromophoric β-(1′-naphthyl)-L-alanine (Nap) residue, and the heavy atom bearing *p*-bromo-L-phenylalanine (Bph) residue. These octameric peptides were *sequence isomers* of each other, with identical compositions (see sequences below), and were designed such that the chromophore and the perturber were separated by two Aib residues (Br-3,6-Oct) or one Aib residue (Br-3,5-Oct) or they occurred as consecutive residues in the peptide sequence (Br-4,5-Oct). The corresponding set

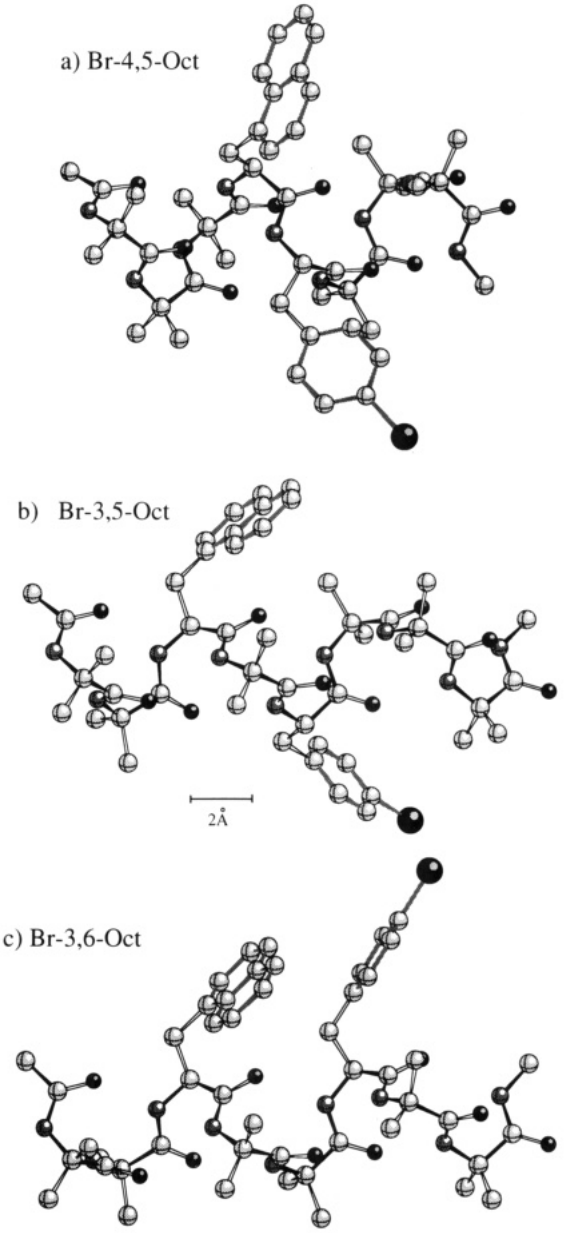

FIGURE 1: Experimentally observed secondary structures for the three sequence isomeric octamers. The peptide backbone (dark) and the two interacting aromatic residues (shaded bonds) are highlighted. The dark atoms are carbonyl oxygens, while the large dark atom represents the bromine atom. Two peptides, Br-3,5-Oct (b) and Br-3,6-Oct (c), display a 3_{10}-helical conformation ($i \leftarrow i+3$ hydrogen-bonding pattern), while the Br-4,5-Oct (a) peptide exhibits an α-helical conformation ($i \leftarrow i+4$ hydrogen-bonding pattern). Note that the Br-4,5-Oct α-helix is shorter and fatter. The Aib-rich octamers are arranged in increasing order of sequence separation: 4,5-Oct < 3,5-Oct < 3,6-Oct. The through-space distances of these peptides increase in a different order [3,6-Oct < 4,5-Oct $\lesssim$ 3,5-Oct], as modulated by the pitch of the helix. This nonmonotonic correspondence between through-space and through-bond distances is the characteristic feature of these helices.

of control peptides for the optical studies, C-3,6-Oct, C-3,5-Oct, and C-4,5-Oct, was prepared, and these peptides are identical to the bromo octamers except that the Bph residue was replaced by the corresponding non-heavy atom residue L-phenylalanine (Phe).

This set of sequence isomeric octamers is designed specifically to address the question of pathways of electronic interactions. While the helical stability of the backbone remains unchanged throughout the series, the TB separation increases monotonically from Br-4,5-Oct to Br-3,6-Oct,

peptides	sequence
Br-3,6-Oct	Ac-(Aib)(Aib)(**Nap**)(Aib)(Aib)(**Bph**)(Aib)(Aib)-NHMe
Br-3,5-Oct	Ac-(Aib)(Aib)(**Nap**)(Aib)(**Bph**)(Aib)(Aib)(Aib)-NHMe
Br-4,5-Oct	Ac-(Aib)(Aib)(Aib)(**Nap**)(**Bph**)(Aib)(Aib)(Aib)-NHMe
C-3,6-Oct	Ac-(Aib)(Aib)(**Nap**)-(Aib)(Aib)(***Phe***)-(Aib)(Aib)-NHMe
C-3,5-Oct	Ac-(Aib)(Aib)(**Nap**)-(Aib)(***Phe***)-(Aib)(Aib)(Aib)-NHMe
C-4,5-Oct	Ac-(Aib)(Aib)(Aib)(**Nap**)(***Phe***)(Aib)(Aib)(Aib)-NHMe

whereas the TS separation between the interacting aromatics is shortest in Br-3,6-Oct followed by a longer distance in Br-4,5-Oct and the longest distance in Br-3,5-Oct. Furthermore, in Br-3,5-Oct and Br-4,5-Oct, the systematic network of H-bonds along the peptide backbone is spatially intermediary between the two chromophores whereas in Br-3,6-Oct the two chromophores face the same side of the helix, so that they are separated by solvent. This structural variation of the intervening medium between the two partners is an advantage relative to the end-capped spacer design and allows one to test whether the exchange interactions in a helical peptide series follow an exponential distance dependence. These helices serve as models of helical proteins where the intervening medium is inherently structured, and simple models based on uniform intervening medium or uniformly bonded linkages may not apply.

Fluorescence quenching experiments were performed on these sets of octameric peptides to study the electronic interaction between the bromophenyl and naphthyl groups in these structures. The solution structures were also probed by ^{1}H NMR. Time-resolved triplet–triplet absorption experiments were then used to reveal the mechanism of the fluorescence quenching by measuring the corresponding changes in triplet yield (ϕ_T). Significant fluorescence quenching of the Nap chromophore was observed in all of the peptides which was partly Nap T_1-producing due to the RHAE and partly non-triplet-producing due to spin-forbidden excitation transfer to the bromophenyl T_1 state. The triplet-producing fluorescence quenching was very effective at a close distance, and its behavior with increasing sequence separation is the central focus of this article. Triplet-producing fluorescence quenching was found to be operative for all three of the bromophenyl-containing peptides, and the observed distance dependence does not correlate with either a simple TS or a TB model. A possible role of hydrogen bonding in the enhancement of the RHAE interaction is also considered.

MATERIALS AND METHODS

Materials. All peptides studied were synthesized by solution-phase methods. The sterically hindered coupling between the Aib residues was achieved by reacting Fmoc-(Aib)-OH with the highly N-activated 2-(dimethylamino)-3,3-dimethylazirine or by the oxazolone route. Suitably N-protected amino acids (Phe, Nap, or Bph) were then coupled to the C-terminal Aib fragments by peptide coupling agents (IIDQ, TBTU, and morpho-CDI) or by the acid chloride method. Further N-protected amino acid residues were coupled to the growing peptide one at a time until reaching the final N-terminal Aib block, which was brought in as a presynthesized block. A detailed synthetic protocol for the octamer C-3,6-Oct has been described elsewhere (Basu et al., 1991), and all of the other octamers were synthesized by variations within this general synthetic strategy.

The peptides were purified by flash chromatography (CH_3OH/CH_2Cl_2) and fully characterized by ^{1}H NMR along the synthetic route. After the final step, they were purified prior to all optical studies by reversed-phase C_{18} HPLC on a Waters Delta-Pak column with 5–20% H_2O in CH_3OH as eluent. The molecular mass and the amino acid sequence were both verified by FAB mass spectrometry, and the FAB-MS data for the bromo octamers are summarized in Table I.

^{1}H NMR Studies. Temperature dependence of amide chemical shifts in DMSO-d_6 and solvent titrations in CD_3CN as a function of added DMSO-d_6 were performed for the three control octamers, C-3,6-Oct, C-3,5-Oct, and C-4,5-Oct, as detailed elsewhere (Basu et al., 1991). The 2D NOESY experiment does not provide useful cross peaks for a peptide of this molecular weight range due to the unfavorable rotational correlation time. Instead, a 2D ROESY experiment (Bothner-By et al., 1984) was performed on C-3,6-Oct in DMSO-d_6, and the experimental conditions have been reported elsewhere (Basu & Kuki, 1992b).

Optical Studies. UV–vis spectra were measured on a Varian DMS-300 spectrophotometer. Steady-state fluorescence emission spectra were measured on a SLM 8000 fluorescence spectrophotometer; all samples were excited at 290 nm with 2-nm excitation and 8-nm emission slit widths. Solvents used for optical studies were of HPLC grade and were used as received. The concentrations of the peptides were measured by diluting a stock solution and monitoring the optical density of the naphthalene chromophore at 284 nm. The final concentrations used were 20 μM or less (OD $\sim$0.1–0.15 at 290 nm). All samples were degassed by at least three freeze–pump–thaw cycles before any yield measurement was taken. Fluorescence spectra (corrected for the lamp output) were used to measure the relative fluorescence quantum yield of the peptides. Since the emission spectra were identical in shape in all of the molecules studied, the relative quantum yields are reported from the corresponding ratios of the emission maxima (340 nm) corrected for the ratio of $(1-10^{-A_{290}})$.

Triplet yields (ϕ_T) were measured with a nanosecond transient absorption spectrometer. The transient absorption measurements were performed with excitation of the sample in a 10 × 10 mm quartz freeze–pump–thaw cuvette with a 290-nm, 5-ns pulse from the doubled output of a dye laser (Rhodamine 610) pumped by the second harmonic of a Q-switched Nd^{3+}:YAG (Quanta-Ray DCR-4 or DCR-2), and with a perpendicular geometry for the xenon arc lamp probe beam. The transmitted beam was detected by a photodiode

Table I: FAB Mass Spectrometric Data for All of the Bromo Octamers

peptides	observed mass of peptide fragments[a] (expected mass of peptide fragments)							
Br-3,6-Oct	213.0	410.0	495.0	580.0	805.0	890.1	975.1	1006.1
	(213.1)	(410.2)	(495.2)	(580.3)	(805.3)	(890.4)	(975.4)	(1006.5)
Br-3,5-Oct	213.1	410.1	495.2	720.2	805.0	890.2	975.8	1006.6
	(213.1)	(410.2)	(495.2)	(720.2)	(805.3)	(890.4)	(975.4)	(1006.5)
Br-4,5-Oct	213.1	298.1	495.1	720.1	805.2	890.2	975.4	1006.5
	(213.1)	(298.2)	(495.2)	(720.2)	(805.3)	(890.4)	(975.4)	(1006.5)

[a] The fragmentation pattern was used to analyze the mass and the sequence for the peptides. The calculated/observed mass is reported only for the fragments corresponding to the ^{79}Br isotope. Fragments for the ^{81}Br isotope were observed as expected.

(EG&G FND100Q) amplified with a fast op-amp (Comlinear CLC-205), and the signal was recorded on a transient digitizer (LeCroy 9450) with averaging capabilities before transfer to a computer for data analysis. An interference filter (10-nm bandpass) was used to filter the probe beam in measurements at the triplet–triplet absorption maximum (420 nm) of the naphthalene chromophore. The naphthalene triplet yields were measured from the amplitude of the triplet–triplet absorption during the first microsecond, prior to any triplet decay. All three control octamers exhibited identical triplet yields (relative to the 1-methylnaphthalene standard), and all triplets measured exhibited the second-order decay kinetics characteristic of triplet–triplet annihilation (>50 μs) of aromatic peptides in degassed room-temperature solution. Thus, structurally revealing triplet quenching, as has been exploited in other biomolecular studies (Vanderkooi et al., 1990), is not observed here.

RESULTS AND DISCUSSION

Solution Conformation of the Octamers. The sequence isomeric octamers were designed to be helical so that variation of the sequence position of the two guest residues would result in a systematic twisting of the partners about the helix axis. Synthetic hydrophobic α-helical peptides are typically designed by the use of long sequences dominated by mono-α-alkylated amino acids with high intrinsic α-helical preference, such as polyglutamate (Sisido et al., 1989). The di-α-alkylated amino acid Aib is rather unique in conferring very high helicity onto short (~8–10 residues) hydrophobic peptides since the α,α-dimethyl group produces a distinctive and thoroughly documented steric strain around C^{α}, such that the conformational space (ϕ,ψ) of backbone torsional angles is severely restricted to the helical region. Either an α-helical ($\phi = -55°$, $\psi = -45°$) or 3_{10}-helical ($\phi = -60°$, $\psi = -30°$) conformation is found, depending upon the exact percent Aib content and the length of the peptide (Karle & Balaram, 1990; Marshall et al., 1990). For peptides containing about 50% Aib, the 3_{10}-helix is known to be favored when the number of residues remains small (<8 residues), whereas when the number of residues exceeds this critical length the α-helix is favored. The number of residues in this critical $3_{10} \rightarrow \alpha$ transition length becomes larger for higher Aib content (>50%) and shorter for lower Aib content (<50%). With this empirical information at hand we designed our peptides, 8 residues long, to contain 75% Aib so that the backbone acquires a 3_{10}-helical conformation. The N-terminal blocking group, acetyl, provided an extra carbonyl, and the C-terminal blocking group, methyl amide, provided an extra amide hydrogen for participation in the intrapeptide H-bonding scheme. In addition, the guest amino acids in the series were always positioned at least two residues in from the peptide termini, ensuring their full participation (of both their amide and carbonyl) in the intrapeptide H-bonding scheme.

The detailed description of the ^{1}H NMR studies performed on the three control octamers has been reported earlier (Basu et al., 1991; Basu & Kuki, 1992b), and in this section a summary of the results relevant to the current work will be presented. The temperature perturbation and the DMSO-d_6 solvent titration studies performed for the backbone amide protons showed that, in CD_3CN, the C-4,5-Oct assumed an α-helical H-bonding pattern. The other two octamers, C-3,6-Oct and C-3,5-Oct, on the other hand, assumed the 3_{10}-helical H-bonding pattern. Our results confirmed the established empirical rules with the exception of a hitherto unobserved $3_{10} \rightarrow \alpha$ transition upon sequence permutation that was attributed to the contiguous presence of two monoalkylated residues in the sequence of C-4,5-Oct (Basu & Kuki, 1992a). With respect to the current work, the resolution of the peptide backbone as either 3_{10}- or α-helical becomes most significant for a peptide where the two interacting residues occur at the $i,i+3$ position, such as Br-3,6-Oct. As a 3_{10}-helix (3.0 residues per turn), the two residues are exactly one turn away from each other and face the same side of the helix, allowing maximum direct interaction. Were it to fold instead into an α-helix (3.6 residues per turn), the residues would not face each other and the possibility for the predominance of a direct interaction at near van der Waals contact would be diminished. The 3,6-octamer was found to be 3_{10}-helical, and therefore the peptide design in the 3,6-octamer not only exploits the helical backbone but uses the unique capability of a 3_{10}-helix to bring two groups exactly one turn apart—a characteristic not shared by the α-helix, the more ubiquitous helix in nature.

For one of the octamers, C-3,6-Oct, direct geometric information about the backbone conformation was obtained from 2D ROESY experiments. A rare pattern of uninterrupted NN($i,i+1$) cross peaks throughout the entire sequence of the octamer was observed (starting from the Aib amide at the N-terminus through the C-terminal blocking amide NHMe), as shown in Figure 2a. Such NN($i,i+1$) cross peaks are characteristic of helical stretches of peptide backbone (this and all other characteristic helical cross peaks are given in Wuthrich (1986)) and for the present case demonstrated the helical backbone conformation of the Aib-rich peptide. In addition, this observation points out the extreme stringency imposed on the helical dihedral angles by the Aib residue since such uninterrupted NN($i,i+1$) cross peaks have previously been observed only in synthetic helical peptides that are almost double the length (Bradley et al., 1990) of C-3,6-Oct. Similar direct information from 2D NOE experiments was not previously available for Aib-containing peptides, and this observation of helical correlations for *every* amide proton clearly distinguishes Aib-rich short peptides as possessing a helical backbone of unusual stability throughout the entire sequence, including the termini.

In addition, the ROE data allowed us to sequence-assign all of the amide protons (Basu & Kuki, 1992b). Combined with the 1D perturbation experiments described earlier, the only two amide protons found to be not intramolecularly 3_{10}-H-bonded are those of Aib_1 and Aib_2 (from the N-terminal), which agrees completely with the 3_{10}-H-bonding scheme. The assignment thus identifies the seven amide protons (Nap through NHMe) participating in the intrahelical H-bonding scheme, and hence H-bonding extends completely to the NH of the C-terminal protecting group and to the carbonyl of the N-terminal protecting group. An additional αN($i,i+3$) cross peak between the Nap and the Phe residue, a characteristic of a helical backbone (both α and 3_{10}), was observed, which independently confirms the helical conformation in the stretch between the two guest residues. Additional evidence on the question of whether the backbone is α- or 3_{10}-helical is provided by the observation of the αN($i,i+2$) cross peaks. The αN distances (in angstroms) in a 3_{10}-helix and an α-helix are given as follows:

	$d_{\alpha N(i,i+2)}$	$d_{\alpha N(i,i+3)}$	$d_{\alpha N(i,i+4)}$	$d_{NN(i,i+2)}$
α-helix	4.4	3.4	4.2	4.2
3_{10}-helix	3.8	3.3	>4.5	4.1

The αN($i,i+3$) and NN($i,i+2$) cross peaks are similar in both helices, whereas the relative strengths of the αN($i,i+2$) and αN($i,i+4$) cross peaks can clearly differentiate the two helices.

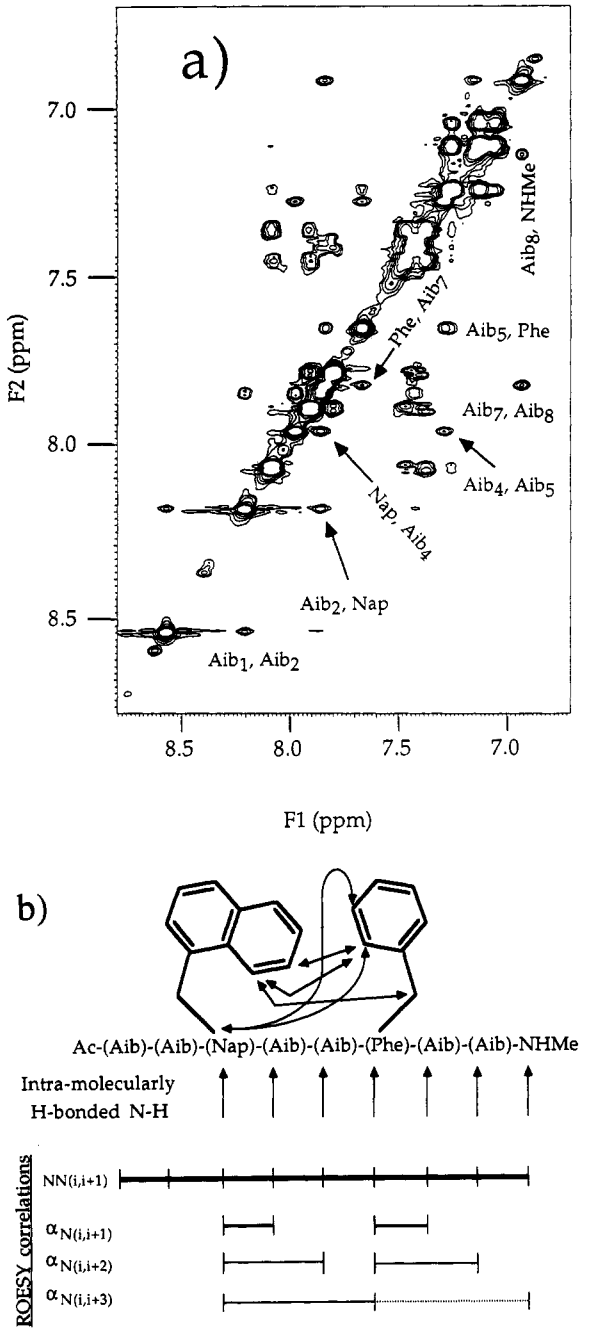

FIGURE 2: Observed NN(i,i+1) ROESY cross peaks (a). Uninterrupted NN(i,i+1) cross peaks observed throughout the sequence of the peptide verify the high degree of helocity of the short but Aib-rich sequence. Summary of all of the observed ROESY cross peaks for C-3,6-Oct in DMSO (b). Additional evidence for the 3_{10}-helical backbone is given by the αN(i,i+3) and αN(i,i+2) cross peaks.

We observed the αN(i,i+3) cross peak, yet the NN(i,i+2) cross peaks were absent (both of these cross peaks are expected in NOESY for either of the two helices). This established that distances longer than 4 Å were beyond the detection limit of the ROESY experiment. If the backbone were α-helical, then neither the αN(i,i+4) cross peak nor the αN(i,i+2) cross peak should have been observed. On the other hand, in a 3_{10}-helical backbone weak αN(i,i+2) cross peaks should be observed. Additional evidence for a 3_{10}-helical geometry was thus obtained from the weak but observable αN(i,i+2) cross peaks. Only two such cross peaks can occur for this peptide (only two residues have C^{α}-H), and both were observed. The 2D ROESY experiments, summarized in Figure 2b, thus reinforced the 3_{10} conformational assignment from the DMSO-d_6 solvent titration experiments and provided direct evidence of the 3_{10}-helical geometry for C-3,6-Oct.

Table II: Fluorescence Yield and Triplet Yield Data for Bimolecular Fluorescence Quenching of 1-Methylnaphthalene

quencher	[Q] (M)	ϕ_F/ϕ_{F_0}	ϕ_T/ϕ_{T_0}
bromobutane	0.0	1.00	1.0
	0.18	0.35	1.32
	0.69	0.13	1.52
	1.28	0.09	1.60
bromobenzene	0.0	1.00	1.0
	0.07	0.25	1.0
	0.14	0.16	0.96
	0.20	0.11	0.93
	0.29	0.08	0.87

Bimolecular Behavior: The Nature of Heavy Atom Perturbation by Bromobenzene. The mechanistic analysis of the RHAE in the peptides requires the determination of several key parameters controlling the behavior of bromobenzene (BrBz) as a heavy atom perturber. Therefore bimolecular fluorescence quenching of 1-methylnaphthalene (MNap) was studied in acetonitrile with bromobutane and bromobenzene as the quenchers. The quenching constants, k_n, obtained from the Stern–Volmer analysis,

$$(\phi_{F_0}/\phi_F) = 1 + k_n\tau_{F_0}[Q] \quad (1)$$

were not diffusion controlled, and hence they reflect the relative intrinsic quenching ability (1.5×10^8 M^{-1} s^{-1} for bromobutane and 6.0×10^8 M^{-1} s^{-1} for BrBz). Exciplex emission was not observed to accompany fluorescence quenching for any of the above-mentioned pairs.[2]

These results are summarized in Table II along with the measured values of ϕ_T/ϕ_{T_0} that accompanied the fluorescence quenching. For the MNap/bromobutane pair, as ϕ_F/ϕ_{F_0} decreased successively, ϕ_T/ϕ_{T_0} values increased (see Table II), which demonstrates that bromobutane is a triplet-producing fluorescence quencher. On the other hand, for the MNap/BrBz pair, the ϕ_T/ϕ_{T_0} distinctly decreased with decreasing ϕ_F/ϕ_{F_0}. This decreasing trend in ϕ_T/ϕ_{T_0}, and the fact that ϕ_T/ϕ_{T_0} and ϕ_F/ϕ_{F_0} are never equal to each other, demonstrates the role of BrBz as a quencher that acts both as a triplet-producing and as a non-triplet-producing fluorescence quencher. This point is elaborated below, and the ratio of the rate constants for the two quenching processes, triplet-producing and non-triplet-producing, is extracted from the analysis of the data.

The quenching of the MNap S_1 excitation by BrBz can lead to the population of either the MNap T_1 or some other state which lies below the MNap S_1. If the fluorescence quenching proceeds by an exclusively non-triplet-forming mechanism, then it follows that

$$\phi_F/\phi_{F_0} = \phi_T/\phi_{T_0} \quad (2)$$

On the other hand, if the fluorescence quenching is exclusively triplet-forming, we have

$$\phi_T/\phi_{T_0} = [(k_t + k^\circ_{ISC})/(k^\circ_{ISC})]/[(k_t + k^\circ_{ISC} + k^\circ_F)/(k^\circ_{ISC} + k^\circ_F)] \quad (3)$$

where k_t is the new triplet-forming quenching rate constant, and k°_F, and k°_{ISC} are the native radiative and unimolecular intersystem crossing rate constants, respectively (the internal conversion rate constant is minor and is set to zero). In this

[2] The exciplex emission for the MNap/BrBz pair previously reported by us (Basu et al., 1990) is attributed to an impurity in the BrBz used.

case, it follows that the fraction of quantum yield which flows through the new quenching pathway enhances the triplet yield:

$$\phi_T/\phi_{T_0} > 1 \quad (4)$$

Experimental data in Table II clearly show that neither of the above two conditions, eq 2 or 4, is satisfied in the bimolecular quenching studies of MNap by BrBz. Therefore, there are at least two Nap S_1 quenching mechanisms present, one triplet-producing and one non-triplet-producing. We write that the new BrBz-induced quenching constant k_n has two components, $k_n = k_x + k_t$, where k_x is the rate constant for the non-triplet-producing quenching and k_t is the rate constant for the triplet-producing quenching. The general formula for the triplet yield, including the k_x and k_t processes, is given below (eq 7). The ratio k_x/k_t may be evaluated in the bimolecular case by use of the following relation (Medinger & Wilkinson, 1965):

$$\phi_{F_0}/\phi_F = 1 + \{(\phi_{F_0}/\phi_F)(\phi_T/\phi_{T_0}) - 1\}\{k_x/k_t + 1\}\phi_{T_0} \quad (5)$$

The fluorescence and triplet yield data plotted as (ϕ_{F_0}/ϕ_F) vs $\{(\phi_{F_0}/\phi_F)(\phi_T/\phi_{T_0}) - 1\}$ provide a k_x/k_t value[3] of 0.75 for the MNap/BrBz pair. Hence we find that $k_t = 3.4 \times 10^8$ and $k_x = 2.6 \times 10^8$ M^{-1} s^{-1} for this pair. See the Appendix for further details. In the following section, we look at these same fluorescence quenching rate processes in the peptides where the interacting partners are held apart, offering the potential for the electronic involvement of the helical frame.

Fluorescence Quenching in the Octameric Peptide Series. All bromine-bearing octamers, Br-3,6-Oct, Br-3,5-Oct, and Br-4,5-Oct, exhibited fluorescence quenching when compared to their corresponding control octamers (Figure 3). The control octamers were identical to within 2% in their fluorescence yields, and the fluorescence quenching for the bromo octamers were not accompanied by any exciplex emission. The results are summarized in Table III. The octamer in which the Nap C^γ and the Bph C^γ were separated by 13 σ bonds (Br-3,6-Oct) showed the maximum quenching of 68%, whereas the other two octamers, Br-3,5-Oct and Br-4,5-Oct, where the C^γ–C^γ through-bond separation was shorter (ten and seven σ bonds, respectively), showed much diminished fluorescence quenching of 11% and 14%, respectively. Clearly the observed fluorescence quenching is not correlated with the direct σ-bonded TB separation in the peptides.

The TS separation between the Nap C^β and the Bph C^β positions in the octamers is modulated by the helical twist and is 5.8 Å for Br-3,6-Oct, 7.3 Å for Br-3,5-Oct, and 5.1 Å for Br-4,5-Oct.[4] The interaromatic edge–edge and center–center distances in Br-3,5-Oct and Br-4,5-Oct are yet longer than this C^β–C^β estimate since in these two peptides the aromatic rings protrude away from each other and out from the helical axis. In Br-3,6-Oct the actual interaromatic distances tend to be shorter than this estimate since the two aromatic rings, facing each other in the same side of the helix, can come quite close by virtue of the sidehchain χ_1 and χ_2 rotations. Therefore, Br-3,6-Oct functionally has the shortest interaromatic TS distance followed by Br-4,5-Oct and then Br-3,5-Oct—this is exactly the trend observed in their fluorescence quenching. The trend that the fluorescence quenching decreases systematically with increasing TS distance seems to suggest that in the octamer series fluorescence quenching is being modulated by TS interaction. However, since the triplet yield ratios accompanying the fluorescence quenching for the octamers (see Table III) do not satisfy eq 2 or 4, there are at least two rate processes responsible for the observed fluorescence quenching just as in the bimolecular quenching case. In order to properly understand the relationship between structure and the observed electronic interactions in the octameric peptide series, it is necessary to analyze independently the two

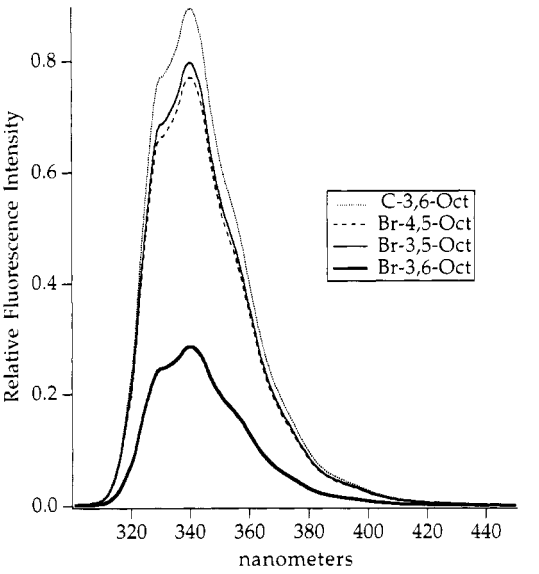

FIGURE 3: Excitation-corrected steady-state fluorescence spectra for the three bromo octamers, Br-4,5-Oct, Br-3,5-Oct, and Br-3,6-Oct, and the control octamer, C-3,6-Oct, in acetonitrile. Relative to the control octamer, all of the bromo octamers exhibit fluorescence quenching; Br-3,6-Oct has the maximum quenching (68%), whereas the other two octamers, Br-4,5-Oct and Br-3,5-Oct, exhibit moderate quenching (14% and 11%, respectively).

Table III: Fluorescence Yields, Triplet Yields, and the Relative Contributions from Triplet-Yielding (k_t) and Non-Triplet-Yielding (k_x) Quenching Rate Constants for the Isomeric Octamers

peptides	ϕ_F/ϕ_{F_0}[a]	ϕ_T/ϕ_{T_0}[a]	k_n[b] (μs^{-1})	k_x[b] (μs^{-1})	k_t[b] (μs^{-1})
Br-4,5-Oct	0.86 ± 0.02	0.91 ± 0.03	2.7 ± 0.4	2.2 ± 0.4	0.5 ± 0.3
Br-3,5-Oct	0.89 ± 0.02	1.01 ± 0.03	2.1 ± 0.4	0.9 ± 0.3	1.1 ± 0.3
Br-3,6-Oct[c]	0.32 ± 0.01	0.85 ± 0.02	35.4 ± 2	21.3 ± 1	14.1 ± 1

[a] These numbers are relative to that of the control octamer C-3,6-Oct. The errors reported in this and all other columns are the standard deviations of the mean. [b] The values for the new quenching constant k_n and for k_t and k_x are obtained from eqs 6 and 8. The error of k_x is properly propagated through the relation: $k_x = [\tau_{F_0}^{-1} - k^\circ_{ISC}(\phi_T/\phi_{T_0})]/(\phi_F/\phi_{F_0}) - (\tau_{F_0}^{-1} - k^\circ_{ISC})$. [c] In the case of Br-3,6-oct, time-resolved fluorescence studies reveal a nonsingle exponential decay. The dominant component has a lifetime of 26.6 ns, which by itself corresponds to $\phi_F/\phi_{F_0} = 0.43$. Here we rigorously define effective $\tilde{k}_n$, $\tilde{k}_t$, and $\tilde{k}_x$ as $\tilde{k}_n \equiv \langle\tau_{F_i}\rangle^{-1} - k_F^\circ - k_{ISC}^\circ$, $\tilde{k}_t \equiv \langle k_t\tau_{F_i}\rangle/\langle\tau_{F_i}\rangle$, and $\tilde{k}_x = \tilde{k}_n - \tilde{k}_t$. These have been defined as the weighted averages over components i such that the basic relations remain exact; a little algebra shows that $\tilde{k}_n = [(\phi_{F_0}/\phi_F) - 1]/\tau_{F_0}$ and $\tilde{k}_t = k^\circ_{ISC}[(\phi_{F_0}/\phi_F)(\phi_T/\phi_{T_0}) - 1]$, and eq 5 is still valid with $(k_x/k_t + 1)$ replaced with $(\tilde{k}_x/\tilde{k}_t + 1)$. These effective rate constants are the rate constants for an equivalent perfectly homogeneous kinetic scheme. The values of $\tilde{k}_n$, $\tilde{k}_t$, and $\tilde{k}_n$ are given above in the table for Br-3,6-Oct.

[3] A knowledge of the absolute triplet yield, ϕ_{T_0}, for the unquenched chromophore is necessary and was obtained from bimolecular fluorescence quenching and the corresponding change in triplet yield for MNap/bromobutane in acetonitrile. The measurement of relative yields with bromobutane (Table II) enables eq 5 to be directly solved for the absolute yield, ϕ_{T_0}. Since it has been established that only enhanced intersystem crossing occurs as the mechanism of fluorescence quenching in this alkyl bromide case, $k_x/k_t = 0$, and a plot of (ϕ_{F_0}/ϕ_F) vs $\{(\phi_{F_0}/\phi_F)(\phi_T/\phi_{T_0}) - 1\}$ will have a slope equal to the absolute triplet yield. We obtain the triplet yield of MNap to be 0.63, which also correctly yields 1 when added to the MNap fluorescence yield (Reiser & Wright, 1973).

[4] These C^β–C^β distances are calculated for the energy-minimized structures of the corresponding octamers shown in Figure 1; these computed structures are also consistent with the experimentally determined solution conformations described in the text.

contributing quenching mechanisms, along with the nature of the electronic interactions responsible for each. In the next section we take up this question in a quantitative fashion.

Rate Processes and Electronic Interactions Associated with Fluorescence Quenching in the Octameric Peptide Series. The changes in triplet yield ϕ_T/ϕ_{T_0} accompanying the fluorescence quenching were measured for the octamers and are shown in Table III. The triplet yields were less than or close to unity relative to that of the control octamers. The magnitude of the new fluorescence quenching rate constant k_n is given by

$$k_n = (\tau_{F_0})^{-1}\{(\phi_{F_0}/\phi_F) - 1\} \quad (6)$$

From the general expression of the triplet yield ratio,

$$(\phi_T/\phi_{T_0}) = [(k_t + k^\circ_{ISC})/(k^\circ_{ISC})]/[(k_t + k_x + k^\circ_{ISC} + k^\circ_F)/(k^\circ_{ISC} + k^\circ_F)]$$
$$= [(k_t + k^\circ_{ISC})/(k^\circ_{ISC})]/(\phi_{F_0}/\phi_F) \quad (7)$$

we can derive a simple expression for the triplet-producing rate constant k_t in the intramolecular case,

$$k_t = k^\circ_{ISC}\{(\phi_{F_0}/\phi_F)(\phi_T/\phi_{T_0}) - 1\} \quad (8)$$

Therefore, with a knowledge of k°_{ISC}, ϕ_{F_0}/ϕ_F, and ϕ_T/ϕ_{T_0}, one can separate the rate constant k_n into its constituents, k_t and k_x (= $k_n - k_t$), by use of eq 8. These individual rate constants are reported in Table III.

The assignment of the kinetic processes k_t and k_x detected in the fluorescence and triplet yield experiments to the specific molecular mechanisms responsible can be made by careful extrapolation from the known behavior of the BrBz quencher in the bimolecular mode. From a consideration of the known photophysics (documented in the Appendix), we propose the mechanisms to be (1) an enhanced ISC within the Nap chromophore due to the remote heavy atom in Bph, which gives rise to the triplet-producing fluorescence quenching (k_t = k_{RHAE}), and (2) a nominally spin-forbidden irreversible energy transfer from the singlet of Nap to the triplet of Bph (k_x = k_{ST}), which proceeds by a very weak dipole–dipole mechanism.

The second process, singlet–triplet energy transfer from Nap S_1 to BrBz T_1, in principle opens up the possibility of another conceivable pathway of Nap triplet production: (3) a Dexter type T_1(BrBz) → T_1(Nap) back energy transfer (k_{TT}) where part of T_1(BrBz) generated can reappear as T_1(Nap). Considering for the moment this possibility, one would have instead

$$k_t = k_{RHAE} + k_{ST}[k_{TT}/(k_{TT} + k_{T^{Br}})] \quad (9)$$

and

$$k_x = k_{ST}[k_{T^{Br}}/(k_{TT} + k_{T^{Br}})] \quad (10)$$

where $k_{T^{Br}}$ is the lifetime of the BrBz T_1 state. The absolute upper limit to the ratio $k_{TT}/k_{T^{Br}}$ imposed by eqs 9 and 10 is k_t/k_x, which was measured at collisional contact (bimolecular quenching) to be k_t/k_x = 1.34. For the peptides with longer distances of interaction (especially Br-4,5-Oct and Br-3,5-Oct), it follows that $k_{TT}/k_{T^{Br}}$ must be much smaller than unity, since $k_{T^{Br}}$ is distance independent and k_{TT} would fall off rapidly with distance. A very small ratio implies irreversible Nap → BrBz energy transfer. Furthermore, the mechanistic evidence discussed in the Appendix on Nap/BrBz indicates that k_t should be dominated by the heavy atom ISC effect without the need to invoke k_{TT}. Thus we will ignore k_{TT} and consider only the k_{RHAE} and k_{ST} processes.[5]

Distance Dependence. The k_x rate constant, assigned as an S_1(Nap) → T_1(BrBz) energy-transfer process, should exhibit a Förster inverse sixth power distance dependence. Since Förster transfer occurs as a result of the dipole–dipole interaction between the interacting partners but does not involve electron delocalization between them, the intervening medium plays only a minor role (Moog et al., 1984). Examining the k_x values in Table III, one finds that indeed the k_x rate constant is strongest for Br-3,6-Oct and weakest for Br-3,5-Oct. Computed distances between Nap and Bph from these k_x values using the Förster expression (with a calculated value of 3.56 Å for R_0, a τ_{F_0} value of 60 ns, and assuming $\kappa^2 = {}^2/_3$),

$$k_{Förster} = (1/\tau_{F_0})(R_0/R)^6[({}^3/_2)\kappa^2] \quad (11)$$

yields distances that are somewhat short (Br-3,5-Oct: 5.8 Å; Br-4,5-Oct: 4.8 Å; Br-3,6-Oct: 3.2 Å), but the ratios match the expected distances well. Empirically then, the interacting partners are closest in Br-3,6-Oct and furthest in Br-3,5-Oct, as expected from the helical twist.

Now we focus on the more interesting RHAE or k_t process. The distance dependence of the RHAE rate is controlled by the square of the electronic factor which gives rise to the effect. In the remote or indirect coupling case, the electronic factor will consist of more than a single elementary matrix element. We propose that the remote heavy atom effect, giving rise to k_{RHAE}, is an indirect quantum mechanical phenomenon which, within the framework of third-order perturbation theory, can be thought to arise through a series of quantum mechanically intermediate states. Specifically, the net intersystem crossing from the Nap S_1 to Nap T states (either T_2 or T_1) is enhanced by the strong native internal heavy atom effect in Bph via two virtual energy-transfer processes: (i) Nap S_1 → Bph S_1 virtual energy transfer; (ii) Bph S_1 → Bph T_1 heavy atom enhanced spin–orbit coupling; and (iii) Bph T_1 → Nap T virtual energy transfer. Note that the virtual energy-transfer processes need not be energetically downhill. The overall RHAE electronic factor will then be proportional to the product of the three constituent matrix elements. Of the three concerted quantum mechanical processes responsible for k_{RHAE}, it is the two virtual energy-transfer contributions, Nap S_1 → Bph S_1 (dipole–dipole) and Bph T_1 → Nap T (electron exchange), which together control the distance dependence for k_{RHAE}. The predicted distance-dependent factor in the rate expression is then the product of the known Förster inverse sixth power distance dependence multiplied by that of the interchromophoric Dexter type electron exchange:

$$k_t = k_{RHAE} \propto |\langle H_{Förster}\rangle\langle H_{Dexter}\rangle|^2 \propto r_{TS}^{-6}|\langle H_{Dexter}\rangle|^2 \quad (12)$$

Rate constants involving Dexter exchange matrix elements

[5] Experimental values for the triplet lifetime of BrBz T_1 would be desirable. Unfortunately, the experimental numbers available for $k_{T^{Br}}$ are very ambiguous (Loeff et al., 1970; Perkampus & Vollbrecht, 1970), possibly because of the reactive nature of the singlet precursor to the BrBz T_1. If the triplet lifetime is longer than ~10 μs *and* k_{TT} is operative, then we should have observed leakage into Nap triplet from Bph triplet over a period of tens of microseconds. Since that was not the observed case, we believe that triplet formation from a back energy transfer mechanism is not occurring in these molecules. Furthermore, the triplet yield ratios are measured from the transient absorption at 1 μs, and hence the analysis need only retain prompt triplet-yielding rate processes.

(matrix elements are denoted as $\langle H \rangle$) tend to fall off exponentially with distance *in an unstructured homogeneous medium* such as organic solvent or frozen glass. In the case of the intrahelical peptide results, the detailed pattern of Förster type interaction, $\langle H_{\text{Förster}} \rangle$, in the helical peptides can be obtained directly from the observed k_x rate. Thus by contrasting the patterns of k_t and k_x variation, the dependence of the Dexter exchange coupling, $\langle H_{\text{Dexter}} \rangle$, upon the structure of these helical peptides can be revealed.

It is striking (see Table III) that k_t does not follow the trend of k_x nor does it exhibit a monotonic dependence on either sequence separation or TS separation. The sequence of effective distances, Br-3,6-Oct < Br-4,5-Oct < Br-3,5-Oct, observed for k_x is interpreted as the TS distance trend. The one-turn separation peptide, Br-3,6-Oct, exhibits the strongest k_t and k_x by an order of magnitude, so that it is evident from this dramatic result that a shorter TS separation strongly enhances all of the electronic interaction terms. But the observation that the k_t rate is faster in Br-3,5-Oct than in Br-4,5-Oct is certainly surprising (note that this cannot be inferred from the comparison of the fluorescence yield data alone). The source of the distinct pattern in k_t is clearly the virtual Dexter electronic interaction term in k_t since the virtual Förster electronic interaction term should follow the observed k_x behavior, which behaves quite consistently with the direct separation distance between the Nap and the Bph residues. In Br-3,5-Oct, where the direct distance of interaction is longer than in Br-4,5-Oct, the Dexter type electronic interaction is nevertheless found to be stronger. If we consider the ratio k_{RHAE}/k_{ST}, which is approximately proportional to the square of the Dexter type electronic contribution, Br-3,5-Oct (k_t/k_x = 1.2) exhibits a greater electronic exchange coupling (by a factor of $(1.2/0.23)^{1/2} = 2.3$) relative to Br-4,5-Oct (k_t/k_x = 0.23).[6]

From the data on the peptides Br-4,5-Oct and Br-3,5-Oct, we can conclude that for molecules where both direct TB and TS pathways are weak, the intervening peptide medium cannot be successfully modeled as a σ-bonded linker nor as an unstructured homogeneous medium. One possibility is that a combination of many indirect pathways, involving covalent bonds, interactions across van der Waals separations, and hydrogen bonds, may become important. Theoretically it is inescapable that such contributing pathways of electronic interaction would possess signs and thereby give rise to interference, which can amplify the sensitivity to structural details (Beratan, 1986; Liang & Newton, 1992; Gruschus & Kuki, 1992). If that is indeed the case, in what way is the intervening medium in Br-4,5-Oct and Br-3,5-Oct different? One way to look at the difference is to consider the intervening peptide backbone and focus on the well-defined hydrogen-bonding network it supports. In addition to the direct TB and TS pathways present in Br-4,5-Oct and Br-3,5-Oct, we list several alternate and parallel linkages that are a combination of covalent and intrahelical hydrogen bond assisted couplings between the C^{γ} of the Nap and Bph residues.

peptides	covalent only	covalent (H-bond)	relative k_t
Br-4,5-Oct	7 bonds	10(+1), 12(+1), 12(+1) bonds	≡1.0
Br-3,5-Oct	10 bonds	9(+1), 9(+1) bonds	2.2×
Br-3,6-Oct	13 bonds	8(+1), 12(+1), 12(+1) bonds	28×

Clearly, while the direct covalent chain length in Br-4,5-Oct is shorter than that in Br-3,5-Oct, when a combination of covalent and H-bond pathways are considered additional alternate pathways with shorter lengths become available in the latter peptide. This bond-counting pathway approach is just a qualitative construction to characterize how the intervening peptide in Br-4,5-Oct and Br-3,5-Oct may differentially affect electron delocalization between Nap and Bph, ultimately affecting the RHAE interaction. It remains a quantitative issue of quantum molecular modeling, with signed interference, to assess whether the intrahelical hydrogen-bonding network is dominantly responsible for the trends in k_t observed here. The data is surprising in demonstrating a k_t trend which is *inverse* to that expected naively from sequence separation. Thus we surmise from the observed k_t trends and the known geometry of the peptides that, when both direct TS and TB interaction pathways become long-range (long for the heavy atom effect), subtle and interfering factors arising from the specific nature of the intervening medium can become important in controlling exchange-mediated interactions between the remote aromatic partners. Parallel studies on a set of Aib peptide based electron-transfer systems are also underway to detect this electronic delocalization across the same helical framework by measurement of the electron-transfer rate constants.

CONCLUSION

We have designed, synthesized, and measured the fluorescence quenching in a sequence isomeric set of short and strongly helical peptides containing guest aromatic partners and Aib as the host residues. The variation in the peptide sequence is only in the position of the two modified aromatic β-alanine guest residues that interact with each other through both exchange-mediated and dipole–dipole interactions. While the sequence isomeric octamers exhibited dipole–dipole-mediated fluorescence quenching modulated by the through-space distance as expected, the pattern of exchange-mediated fluorescence quenching is incompatible with either a covalent through-bond mechanism or a simple through-space monotonic decay. The helical twist is unambiguously responsible for the fact that Br-3,6-Oct exhibits the strongest remote heavy atom effect of the series. Yet the full three-dimensional geometry of the intervening hydrogen-bonded peptide medium, and not simple one-dimensional measures, must be considered to account for all of the rates measured. The implications for highly folded structures such as proteins are that interactions beyond those arising from a covalent linkage cannot be ignored on the basis of a simpler set of molecules lacking the relevant secondary structural components and that more subtle structural features present in the inhomogeneous protein matrix, such as the network of noncovalent interactions across numerous van der Waals contacts and hydrogen bonds, may contribute significantly.

ACKNOWLEDGMENT

We gratefully acknowledge Matt Kubasik for suggesting several ideas that shaped this work and for obtaining the time-resolved fluorescence data.

APPENDIX

Molecular Mechanisms for the Fluorescence Quenching of the Naphthalene Chromophore by the Bromobenzyl Component. It was established both in the bimolecular studies and in the helical peptides that there must be at least two

[6] A direct determination from the experiment of each individual electronic matrix element requires the estimation of the intrinsic BrBz matrix element as well as the Franck–Condon weighted density of vibrational states to supply other coefficients for eq 12 (Basu et al., 1992).

kinetic processes that are responsible for the quenching of Nap fluorescence by BrBz. The quenching process that concomitantly produces Nap triplet is the remote heavy atom effect (RHAE), the enhancement of the intersystem crossing (ISC) rate of $S_1 \rightarrow T_1$ within the Nap chromophore, which requires the transport of spin-angular momentum between the two interacting aromatic partners. This cannot occur by a dipole–dipole mechanism, but can result through an electron-exchange-mediated interaction with the BrBz moiety. Thus while the RHAE, electron transfer, and Dexter type triplet–triplet energy transfer are quite distinct kinetic processes, their respective rate constants can be written in the usual way (Fermi's golden rule) as a product of an electronic matrix element squared and a vibrational density of states factor, and it is at the level of the common electronic exchange matrix elements that there is a relationship. In electron transfer there is a net change in electron population. In Dexter type triplet–triplet energy transfer there are two virtual electron transfers leading to no net particle movement, yet net transfer of energy and spin-angular momentum. The donor triplet is returned to its electronic ground state. We propose that in the RHAE there are two virtual energy-transfer matrix elements, of which one is the triplet–triplet energy-transfer matrix element (which in turn is related to electron exchange). In the net RHAE process as defined here, there is no net particle movement, yet there is spin-angular momentum transfer and conversion of the electronic energy difference between the Nap S_1 and T_1 states into Nap vibrational energy. The two virtual energy-transfer matrix elements[7] responsible for the RHAE process are shown in the text as the distance-dependent factors in the quantum mechanical rate expression, eq 12. Additional contributing factors are the electronic matrix element for the intrinsic BrBz spin–orbit coupling and the Franck–Condon weighted density of final vibrational states for Nap $S_1 \rightarrow T_1$, which arises due to the conversion of the electronic energy into vibrational excitation.

As seen from the observed values of ϕ_T/ϕ_{T_0}, the RHAE-enhanced ISC must be accompanied by some other process (k_x) that quenches the fluorescence without producing any Nap triplet. The lowest triplet state of BrBz lies below the Nap S_1 state, and thus the S_1(Nap) $\rightarrow$ T_1(BrBz) energy-transfer process, while nominally spin-forbidden in either dipole–dipole or exchange mechanisms, is energetically favorable and becomes a candidate for the second quenching process. Due to the presence of the strong native spin–orbit coupling in bromobenzene, its lowest triplet state acquires partial singlet character which lifts the spin forbiddenness of the S_1(Nap) $\rightarrow$ T_1(BrBz) energy transfer and enables this to participate as the second pathway for fluorescence quenching. The efficiency of both modes of bromobenzene-induced fluorescence quenching, enhanced ISC and energy transfer, can be quantitatively gauged in the following way.

The role of BrBz in enhancing the spin–orbit coupling in chromophores whose fluorescence it quenches is well-known (Medinger & Wilkinson, 1965). This was conclusively proven by the observation of increased ϕ_T as the ϕ_F of anthracene decreased during BrBz addition (here energy transfer is not energetically possible, $\phi_T/\phi_{T_0} > 1$, and the bimolecular quenching constant for this external heavy atom enhanced ISC was 2.5×10^8 M^{-1} s^{-1}). As discussed earlier, the measured values of ϕ_T accompanying bimolecular fluorescence quenching in MNap demonstrate that enhanced ISC is operative in the MNap/BrBz system with a very comparable k_t rate constant of 3.4×10^8 M^{-1} s^{-1}. It is known that naphthalene, like anthracene, is particularly susceptible to external heavy atom induced enhanced ISC (Dreeskamp et al., 1974) because of the small energy gap to an ungerade T_2 state lying only about 1000 cm^{-1} below its S_1 state (Hanson & Robinson, 1965). Independent supporting evidence for the effectiveness of BrBz-induced ISC comes from the comparison of the naphthalene/neat BrBz system with the naphthalene/neat ethyl bromide system (Berlman, 1973), where the pseudo-unimolecular rate of quenching for the first pair is about double (3.5×10^9 and 1.5×10^9 s^{-1}, respectively) that of the latter. Ethyl bromide as an external heavy atom quencher only enhances the ISC process, whereas BrBz in addition quenches the fluorescence by non-triplet production; one can thus estimate that, for the naphthalene/BrBz pair at collisional contact, the enhanced ISC fluorescence quenching rate should be nearly equal to the rate of the non-triplet-producing process, in good accord with the $k_x/k_t = 0.75$ ratio found here.

Energy transfer from the Nap S_1 to the BrBz T_1 is the pathway most likely to be responsible for the non-triplet-producing process observed for these molecules. The triplet of BrBz lies approximately 2700 cm^{-1} below the Nap S_1. Singlet–triplet energy transfer by either Förster (dipole–dipole) or Dexter (exchange) mechanisms is a rare occurrence, although it has been experimentally observed (Lewitzka & Löhmannsröben, 1990) when the triplet involved belongs to a molecule with strong native spin–orbit coupling. The Förster type interaction between the weak emission transition dipole moment of Nap and the extremely weak spin-forbidden absorption transition dipole moment of BrBz was estimated from the Förster overlap integral of the Nap emission and the BrBz $S_0 \rightarrow T_1$ absorption spectra; this yielded 3.56 Å as R_0 (distance at which the energy-transfer efficiency is 50%). Thus, such an energy-transfer process can be effective at close contact and account for the k_x quenching process.

The modulation of these two quenching processes by the peptide structure is reflected in the k_t and k_x data (Table III) where the energy-transfer rate (k_x) follows a predictable pattern, but the RHAE-enhanced ISC (k_t) does not. This reflects the relative insensitivity of the Förster dipole–dipole coupling to the details of the interchromophoric linkage. There is no need to elaborate a separate rate theory for k_x in the peptides. On the other hand, the electron-exchange-dependent RHAE process is qualitatively altered when two interacting aromatics are separated from van der Waals contact out to a distance where they can only interact by an indirect mechanism, requiring intimate involvement of the electrons of the intervening medium. This sensitivity opens the door to a wider and more complex range of structural determinants.

[7] While for most purposes the salient feature of the Föster theory is its inverse sixth power distance dependence, it is also possible to directly evaluate the Förster matrix element itself (Basu et al., 1992).

REFERENCES

Basu, G., & Kuki, A. (1992a) *Biopolymers 32*, 61–71.

Basu, G., & Kuki, A. (1992b) *Biopolymers* (accepted for publication).

Basu, G., Kubasik, M., Anglos, D., Secor, B., & Kuki, A. (1990) *J. Am. Chem. Soc. 112*, 9410–9411.

Basu, G., Bagchi, K., & Kuki, A. (1991) *Biopolymers 31*, 1763–74.

Basu, G., Kubasik, M., Anglos, D., & Kuki, A. (1992) *J. Phys. Chem.* (in press).

Beratan, D. N. (1986) *J. Am. Chem. Soc. 108*, 4321–4326.

Beratan, D. N., Onuchic, J. N., & Gray, H. B. (1991) in *Electron Transfer in Metalloproteins* (Sigel, H., & Sigel, A., Eds.) pp 97–128, Marcel Decker, Inc., New York.

Berlman, I. B. (1973) *J. Phys. Chem. 77*, 562–567.

Bradley, E. K., Thomason, J. F., Cohen, F. E., Kosen, P. A., & Kuntz, I. D. (1990) *J. Mol. Biol. 215*, 607–622.
Broo, A., & Larsson, S. (1991) *J. Phys. Chem. 95*, 4925–4928.
Christensen, H. E. M., Conrad, L. S., Mikkelsen, K. V., Nielsen, M. K., & Ulstrup, J. (1990) *Inorg. Chem. 29*, 2808–2816.
Closs, G. L., Piotrowiak, P., MacInnis, J. M., & Fleming, G. R. (1988) *J. Am. Chem. Soc. 110*, 2652–2653.
DeFelipps, M. R., Faraggi, M., & Klapper, M. H. (1990) *J. Am. Chem. Soc. 112*, 5640–5642.
Dexter, D. L. (1953) *J. Chem. Phys. 21*, 836–850.
Dreeskamp, V. H., Koch, E., & Zander, M. (1974) *J. Phys. Chem. 94*, 2740–2743.
Förster, Th. (1948) *Ann. Phys. (Leipzig) 2*, 55–75.
Gruschus, J., & Kuki, A. (1992) *J. Phys. Chem.* (submitted for publication).
Hanson, D. M., & Robinson, G. W. (1965) *J. Chem. Phys. 43*, 4174–4175.
Inai, Y., Sisido, M., & Imanishi, Y. (1990) *J. Phys. Chem. 94*, 6237–6243.
Isied, S. S., Ogawa, M. Y., & Wishart, J. F. (1992) *Chem. Rev. 92*, 381–394.
Karle, I. L., & Balaram, P. (1990) *Biochemistry 29*, 6747–6756.
Kuki, A. (1991) in *Long-Range Electron Transfer in Biology* (Palmer, G. A., Ed.) pp 49–83, Springer-Verlag, Berlin.
Kuki, A., & Wolynes, P. G. (1987) *Science 236*, 1647–1652.
Lewitzka, F., & Löhmannsröben, H. G. (1990) *Z. Phys. Chem. Neue Folge 169*, 181–202.
Liang, C., & Newton, M. D. (1992) *J. Phys. Chem. 96*, 2855–2866.
Loeff, I., Lutz, H., & Lindquvist, L. (1970) *Isr. J. Chem. 8*, 141–146.
Marshall, G. R., Hodgkin, E. E., Langs, D. A., Smith, G. D., Zabrocki, J., & Leplawy, G. D. (1990) *Proc. Natl. Acad. Sci. U.S.A. 87*, 487–491.
Medinger, T., & Wilkinson, F. (1965) *Trans. Faraday Soc. 61*, 620–630.
Moog, R. S., Kuki, A., Fayer, M. D., & Boxer, S. G. (1984) *Biochemistry 23*, 1564–1571.
Perkampus, H. H., & Vollbrecht, H. R. (1971) *Spectrochim. Acta 27A*, 2173–2189.
Prasad, B. V. V., & Balaram, P. (1984) *CRC Crit. Rev. Biochem. 16*, 307–348.
Reiser, A., & Wright, T. R. (1973) *J. Chem. Phys. 59*, 3433–3434.
Schanze, K. S., & Cabana, L. A. (1990) *J. Phys. Chem. 94*, 2740–2743.
Siddarth, P., & Marcus, R. A. (1990) *J. Phys. Chem. 94*, 8430–8434.
Sisido, M., Tanaka, R., Inai, R., & Imanishi, Y. (1989) *J. Am. Chem. Soc. 106*, 1732.
Toniolo, C., Bonora, G. M., Barone, V., Bavoso, A., Benedetti, E., Di Blasio, B., Grimaldi, P., Lelj, F., Pavone, V., & Pedone, C. (1985) *Macromolecules 18*, 895–902.
Vanderkooi, J. M., Englander, S. W., Papp, S., Wright, W. W., & Owen, C. S. (1990) *Proc. Natl. Acad. Sci. U.S.A. 87*, 5099–5103.
Wüthrich, K. (1986) *NMR of Proteins and Nucleic Acids*, Wiley, New York.